

Multiobjective Ranking and Selection Using Stochastic Kriging

Sebastian Rojas Gonzalez^{a,c,*}, Juergen Branke^b, Inneke Van Nieuwenhuyse^{a,c}

^a*Department of Information Technology, Ghent University, Belgium.*

^b*Department of Operations, Warwick University, United Kingdom*

^c*VCCM Core Lab, Flanders Make and Data Science Institute, Hasselt University, Belgium*

Abstract

We consider multiobjective simulation optimization problems, where several conflicting objectives are optimized simultaneously, and can only be observed via stochastic simulation. The goal is to find or approximate a (discrete) set of Pareto-optimal solutions that reveal the essential trade-offs between the objectives, where optimality means that no objective can be improved without deteriorating the quality of any other objective. The noise in the observed performance may lead to two possible misclassification errors: solutions that are truly Pareto-optimal can be wrongly considered dominated, and solutions that are truly dominated can be wrongly considered Pareto-optimal. We propose a Bayesian multiobjective ranking and selection method to reduce the number of errors when identifying the solutions with the true best expected performance. We use stochastic kriging metamodels to build reliable predictive distributions of the objectives, and exploit this information in two efficient screening procedures and two novel sampling criteria. We use these in a sequential sampling algorithm to decide how to allocate samples. Experimental results show that the proposed method only requires a small fraction of samples compared to the standard allocation method, and it's competitive against the state-of-the-art, with the exploitation of the correlation structure being the dominant contributor to the improvement.

Keywords: Simulation Metamodeling, Stochastic Kriging, Multiobjective Simulation Optimization, Multiobjective Ranking and Selection

1. Introduction

In *multiobjective* or *multi-criteria* optimization problems, the goal is to find the set of decision vectors that reveal the essential trade-offs between the objectives (i.e., where no single objective can be improved without negatively affecting any other objective). The resulting optimal solution vectors are referred to as *non-dominated* or *Pareto-optimal*, and form the *Pareto set*, also referred to as the *efficient set*; the evaluation of these solutions in the objectives corresponds to the *Pareto front* (see Figure 1 for some examples of continuous fronts). Depending on the type of problem, the Pareto front may have different

*Corresponding author

Email address: `sebastian.rojasgonzalez@ugent.be` (Sebastian Rojas Gonzalez)

geometries (e.g. concave, convex, linear, disconnected). In real-life problems, the location and geometry of the Pareto front are evidently unknown, and a discrete set of solutions is often used to approximate it (Miettinen, 1999; Hunter et al., 2019).

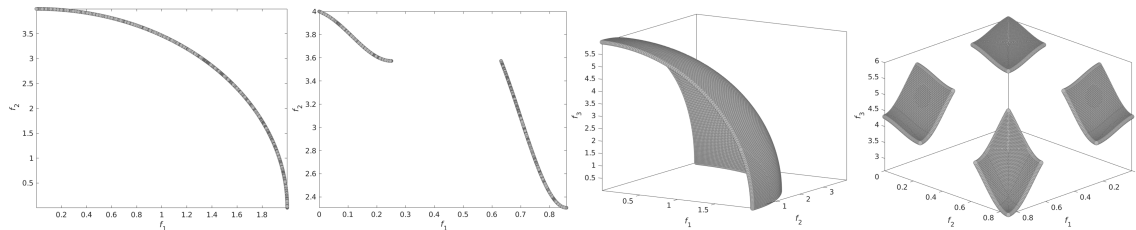


Figure 1: Bi-objective (left) and tri-objective (right) Pareto fronts with different geometries.

Many of today’s real-life decision problems are highly complex, exhibit such multi-objective challenges and tend to be *stochastic*: for a given decision vector, the resulting objective outcomes cannot be observed with perfect accuracy (i.e., they are noisy). For instance, in manufacturing and distribution problems (e.g., lot sizing in manufacturing plants), it is common to maximize the expected profit of the production system, while also minimizing profit risk; in transportation problems (e.g., constructing optimal routes for dial-a-ride services) it is common to minimize tardiness of deliveries while also using minimal resources; and in the healthcare sector it is often equally important to minimize the waiting time of patients and the idle time of doctors.

Often, stochastic simulation is used as a tool to study such systems (see e.g., Kleijnen 2015, Law 2015): the simulation model numerically evaluates the objectives for a given decision vector. Despite its relevance in practice, the current literature on *multiobjective stochastic simulation optimization* is scarce (Hunter et al., 2019). Most of the literature focuses on metaheuristic approaches, such as noisy evolutionary multiobjective optimization algorithms (see e.g., Horn et al. 2017). These have significant shortcomings in settings where the simulation is computationally expensive (i.e., it takes a long time to run a single replication) and/or the decision maker has a limited simulation budget. Ideally, an algorithm should search the solution space in a way that is both effective (having high probability of finding the Pareto-optimal decision vectors), and efficient (using minimal computational budget).

Static resampling (which evaluates each solution a fixed number of times, using the mean of these replications as an approximation of the response value) is the most commonly used method to account for the noise on the performance estimates (Jin & Branke, 2005). However, in settings with limited budget and complex noise structures, this method is likely inefficient, as (1) it may waste a lot of replications on inferior solutions (Rojas-Gonzalez et al., 2020), and (2) the remaining noise levels on the performance estimates may still be such that they prevent the analyst from correctly identifying the Pareto-optimal solutions. It is thus necessary to take into account the noise disturbing the performance during the search (i.e, when sampling new solutions), *and* during the identification of solutions (i.e., when determining the Pareto-optimal set after the search), otherwise, the

algorithm may lead to incorrect inference about the system’s performance.

In the limited literature, the *search* and *identification* problems are often approached separately: in the literature focusing on algorithms to search for solutions (see e.g., Fieldsend & Everson 2015; Hernández-Lobato et al. 2016), the identification phase is often neglected, and the observed sample means are directly used to determine the Pareto-optimal set. On another stream of literature, the focus problem is merely the identification phase, where *after* obtaining a set of competitive solutions, based on the observed performance, *multiobjective ranking and selection* (MORS) methods are used to determine the solutions with the true best expected performance (i.e., to smartly distribute the computational budget only among a subset of critically competitive designs); see e.g., Applegate et al. (2020); Lee et al. (2010); Branke & Zhang (2019). Although ranking and selection methods are standard in single-objective (stochastic) simulation optimization (Kim & Nelson, 2006), the MORS literature is scarce and relatively recent. Preferably, an algorithm should incorporate both phases for solving problems in practice (see Rojas-Gonzalez et al. 2020 for a recent work in this direction).

In this paper we propose a sequential MORS method that has several novel features. Its main advantage is that it uses *stochastic kriging* (SK) metamodels (Ankenman et al., 2010) to build reliable predictive distributions of the objectives, based on the sample means and variances after replication, and thus it is able to exploit correlations between the alternatives. This also allows the proposed method to naturally handle problems with heteroscedastic noise (as opposed to the common homoscedastic assumption in the literature Jal17). As we will show in further sections, another advantage is that it can be paired with other search and/or MORS methods, as the SK predictions are generally better approximations than the sample means. In two novel resampling criteria, we exploit the difference between the SK predictions and the observed sample means (and their respective variances), in combination with an approximation of the recently proposed *expected hypervolume change* (Branke et al., 2016; Branke & Zhang, 2019). In addition, we propose two screening procedures to reduce the computational burden at each iteration. This information is used to determine which points in the solution set should get more replications, in order to improve the identification of the true Pareto-optimal solutions. To the best of our knowledge, this is the first MORS procedure in the literature to implement these aspects; in Rojas-Gonzalez et al. (2019) some preliminary results of the method presented here were published.

The remainder of this article is organized as follows: pending. Section 5.1 explains the two proposed sampling criteria; the proposed algorithm, referred to as SK-MORS, is outlined in Section 5.1.3. We design the experiments to evaluate the performance of the algorithm and the two proposed sampling criteria in Section 6, analyze the results in Section 6.1 and conclude in Section 7.

2. Related work

The ranking and selection problem has been widely studied in the single-objective case, and has been approached in different ways. One of the most common goals is to maximize the *probability of correct selection* (PCS), where under some mild conditions, convergence to the solution with the true best expected performance can be theoretically guaranteed (see e.g., Boesel et al. 2003; Kim & Nelson 2006; Frazier 2014). In some cases, an extremely large replication budget might be required to differentiate two solutions with almost identical performance, and the decision-maker might not consider it a relevant difference. Therefore, *indifference zone* (IZ) approaches have been developed. IZ procedures give a probabilistic guarantee on the selection of the best solution, or a solution within a given user-defined quantity from the best (known as the *probability of good selection*). This user-specified quantity defines the indifference zone, and it represents the smallest difference worth detecting (see e.g., Kim & Nelson 2001; Boesel et al. 2003; Fan et al. 2016).

Relative to the single-objective case, the literature on multiobjective PCS and IZ is scarce (hereafter denoted mPCS and mIZ). The mPCS is defined as the probability of correctly identifying the entire Pareto set, and only this set (Branke & Zhang, 2019). For both the single and multiobjective case the true PCS must be estimated, usually via Monte Carlo simulation, which often leads to a computational bottleneck (Chen & Lee, 2010). In the multiobjective case these exacerbate, as not only the true Pareto front is often continuous and unknown (and thus approximated with a relatively large discrete set), but the dominance relationships between solutions are very sensible to simulation replications due to the trade-off nature between the multiple objectives (see e.g. the results in Rojas-Gonzalez et al. 2020). Very recently, Andradóttir & Lee (2021) proposed a mIZ procedure to estimate the Pareto set with the true best expected performance with statistical guarantees. Even though the method is parametrical, unlike other previous works, it focuses on providing a stopping criterion for replicating designs until a predetermined desired mPCS is achieved, which is desirable in some MORS settings, but at the expense of a large replication budget. Another related work appears in Binois et al. (2015), where by means of kriging metamodels, predictive distributions are built over the objectives and conditional simulations are used to estimate the probability that any given point in the objective space is dominated; the method is found to be very sensible to the (unknown) geometry of the Pareto front, and is computationally expensive. To the best of our knowledge, there are only other two mIZ procedures in the literature: Teng et al. (2010) and Branke & Zhang (2019). The latter work clearly puts in evidence the shortcomings of the first, but remains limited to the biobjective case, and is computationally expensive.

One of the most widely used MORS methods is the *Multiobjective Optimal Computing Budget Allocation* (MOCBA), proposed in Lee et al. (2010); Chen & Lee (2010), built upon the well-known single-objective ranking and selection approach OCBA (Chen & Lee, 2010). As discussed in Lee et al. (2010), the MORS problem can be formulated

in several ways (e.g., maximizing the mPCS or minimizing the classification errors when identifying the non-dominated set). Solving these problems exactly is infeasible, as the true Pareto set is normally unknown. Thus, the computation of the proposed allocation rules is complex, as they depend on numerical approximations of certain parameters: due to stochasticity, a design might be dominated by one design with high probability, but also dominating others with high probability. Thus, non-trivial rules must be devised to determine which roles the designs are playing. In Chen & Lee (2010) a simplified version of the original MOCBA is proposed, which avoids most of these issues; in this work we use this version of the MOCBA allocation rules, stated in Appendix A.

A different approach to the MORS problem is presented in the *SCORE allocations for bi-objective ranking and selection* framework (Feldman et al., 2015; Feldman & Hunter, 2018), which accounts for correlations between the objectives, is asymptotically optimal and aims to allocate replications to maximize the rate of decay of the probability of wrongly identifying the true Pareto set. More recently in Applegate et al. (2020), the work was extended to handle 3 and 4 objectives, showing promising results despite the high computational cost. The recent M-MOBA and M-MOBA-HV frameworks (Branke et al., 2016; Branke & Zhang, 2019) apply a Bayesian perspective to determine the solution that, when replicated further, is expected to yield the maximum *information value* (Chick et al., 2010). In the M-MOBA algorithm, this solution is the one with the highest probability of changing the current Pareto set, whereas in M-MOBA-HV, it is the one leading to the largest change in the observed hypervolume (a widely used metric in multiobjective optimization, that quantifies the volume of the objective space dominated by a given set of points; see Zitzler et al. 2007; Auger et al. 2012 for further details on hypervolume).

Another stream of research is dynamic resampling, which, as its name suggests, dynamically varies the additional number of samples based on the estimated variance of the observed objectives' values. Thus, it allows for the assessment of the observed responses at a particular confidence level before determining dominance, and aims to avoid unnecessary resampling (see e.g., Di Pietro et al. (2004); Syberfeldt et al. (2010)). These methods move away from optimizing a problem in view of converging to the true Pareto set, but rather focus on reducing the variance in the observations, which can be desirable in some practical cases. Another example is the Rolling Tide Evolutionary Algorithm (Fieldsend & Everson, 2015), which instead of using variance learning techniques, it is done during the evolutionary phase of the algorithm, by tracking the improvement on the Pareto set (as opposed to the Pareto front), by focusing on the observation that the best estimate for the noise-free objectives associated with a design improves with the number of samples taken.

Finally, another related problem is to determine the dominance relationships between all the solutions accounting for the noise perturbing their performance (i.e., to provide a statistical guarantee that the observed non-dominated set is within a desired confidence interval). To the best of our knowledge, there is no formal definition in the literature of *stochastic Pareto dominance*; one of the closest attempts is the concept of *probabilis-*

tic dominance, which specifies the minimum probability with which a solution dominates another solution (Fieldsend & Everson, 2005). Thus, instead using outright dominance (see Definition 1), domination is determined using a degree of confidence. Some of the early works that discussed probabilistic dominance appear in Fieldsend & Everson (2005) and Basseur & Zitzler (2006), who propose to use the *expected* values of any deterministic indicator to compare the quality of different Pareto fronts with a certain confidence level, under the assumption that each solution is inherently associated with a probability distribution over the objective space. Zitzler et al. (2008) propose to use non-parametric statistical tests for comparing deterministic indicator values of two or more Pareto fronts. More recently, in Voß et al. (2010), probabilistic dominance is defined by comparing the volume in the objective space of the confidence intervals, and the center point of these volumes is used to determine the dominance relationship. Similarly, in Trautmann et al. (2009), the standard deviation is added to the mean such that dominance is determined with the quantile objective values. The main drawback of these methods is that a design might be dominated by one design with high probability, but also dominating others with high probability (see comments on the MOCBA approach above).

3. Problem definition

The multiobjective optimization problem under output uncertainty can be defined as follows: $\min[f_1(\mathbf{x}, \epsilon_1), \dots, f_m(\mathbf{x}, \epsilon_m)]$, for $m = \{2, 3\}$ objectives; the problem with $m \geq 4$ objectives is known as many-objective optimization, and exhibits several crucial differences to the multiobjective case (Hisao Ishibuchi et al., 2008). The *decision vectors* $\mathbf{x} = [x_1, \dots, x_n]^T$ (also referred to as *solutions* or *designs*) are contained in the decision space \mathcal{X} (usually $\mathcal{X} \subset \mathbb{R}^n$), with $f : \mathcal{X} \rightarrow \mathbb{R}^m$ the vector-valued function with coordinates f_1, \dots, f_m in the objective space $\Theta \subset \mathbb{R}^m$. The observational noise is denoted by $\epsilon_j, j = 1, \dots, m$, and it is commonly assumed to be (i) additive, because it is added to any noise that is extrinsic to the system, and (ii) independent among the different objectives and identically distributed across replications. The noise is commonly assumed to be homoscedastic (see e.g., Koch et al. 2015; Horn et al. 2017; Hernández-Lobato et al. 2016; Zuluaga et al. 2016); that is, the objective values are perturbed with constant noise levels across the search space: $f_j(\mathbf{x}, \epsilon_j) = f_j(\mathbf{x}) + \epsilon_j, j = 1, \dots, m$. In practice, however, the noise is often heteroscedastic (Kim & Nelson, 2006; Ankenman et al., 2010); its level is dependent on the decision variables and thus not constant throughout the search space: $f_j(\mathbf{x}, \epsilon_j) = f_j(\mathbf{x}) + \epsilon_j(\mathbf{x}), j = 1, \dots, m$.

In the *deterministic* case, the Pareto front is obtained by ranking the performance of the solutions using a non-dominated sort, based on Definition 1 (Miettinen, 1999; Deb et al., 2002; Branke et al., 2008):

Definition 1. For \mathbf{x}_1 and \mathbf{x}_2 two vectors in D :

- $\mathbf{x}_1 \prec \mathbf{x}_2$ means \mathbf{x}_1 dominates \mathbf{x}_2 iff $f_j(\mathbf{x}_1) \leq f_j(\mathbf{x}_2), \forall j \in \{1, \dots, m\}$, and $\exists j \in \{1, \dots, m\}$ such that $f_j(\mathbf{x}_1) < f_j(\mathbf{x}_2)$

- $\mathbf{x}_1 \prec \mathbf{x}_2$ means \mathbf{x}_1 strictly dominates \mathbf{x}_2 iff $f_j(\mathbf{x}_1) < f_j(\mathbf{x}_2), \forall j \in \{1, \dots, m\}$.

In the noisy case, the observed performance for each objective is commonly estimated by averaging the value of r_i replications at a given input vector \mathbf{x}_i as $\bar{f}_j(\mathbf{x}_i) = \sum_{k=1}^{r_i} f_j^k(\mathbf{x}_i)/r_i$, $j = 1, \dots, m$, where $f_j^k(\mathbf{x}_i)$ denotes the performance of the k -th observation of \mathbf{x}_i on objective j . These estimates are then directly used to obtain the *observed* Pareto front. Clearly, by relying on the observed mean objective values, we may incur two possible errors due to sampling variability: designs that belong to the true non-dominated set can be wrongly considered dominated, or designs that are truly dominated are considered Pareto-optimal. Moreover, the level and structure of the noise may considerably differ among the objectives, and thus allocating the computational budget becomes non-trivial. Chen & Lee (2010) refer to these errors as *Error Type 1* (MCE) and *Error Type 2* (MCI) respectively, whereas Hunter et al. (2019) refer to them as *misclassification by exclusion* (MCE) and *misclassification by inclusion* (MCI). In the machine learning literature these errors are also widely used in multiple contexts (see e.g., Fawcett 2006; Ting 2017; Powers 2020), and are known as *false negatives* and *false positives*, respectively. Throughout this paper we will continue using the MCE/MCI terminology.

We thus consider the problem of efficiently identifying the designs with the true best expected performance out of a given set of alternatives, when these alternatives are evaluated on multiple (i.e., 2 or 3) stochastic objectives perturbed with heteroscedastic noise. For simplicity, let f_{ij} and σ_{ij}^2 denote the true unknown performance and variance of design i in objective j , respectively; the estimated performance and sample variance after k replications are then denoted \bar{f}_{ijk} and s_{ijk}^2 , respectively. As commonly done in the literature, we assume the performance of a solution in each objective follows a normal distribution and the samples on each objective are independent (Branke & Zhang, 2019):

$$\{X_{ijk} : k = 1, 2, \dots, r_i\} \stackrel{\text{iid}}{\sim} \mathcal{N}(f_{ij}, \sigma_{ij}^2), \forall i = 1, \dots, n; j = 1, \dots, m \quad (1)$$

where X_{ijk} denotes the matrix containing the simulation output for design i , objective j and replication k . The current *observed* Pareto set (i.e., the Pareto set based on sample means) will be determined based on the $r_i, i = 1, \dots, n$ replications so far on each objective. After an additional r'_i simulation replications are performed, yielding an average performance of \bar{f}'_{ij} , the observed mean is updated as:

$$\bar{f}'_{ij} = \frac{r_i \bar{f}_{ij} + r'_i \bar{f}'_{ij}}{r_i + r'_i}. \quad (2)$$

Naturally, the observed Pareto set is also updated, and the dominance relationships among the alternatives will most likely change, and in some cases change drastically (see Figure 2).

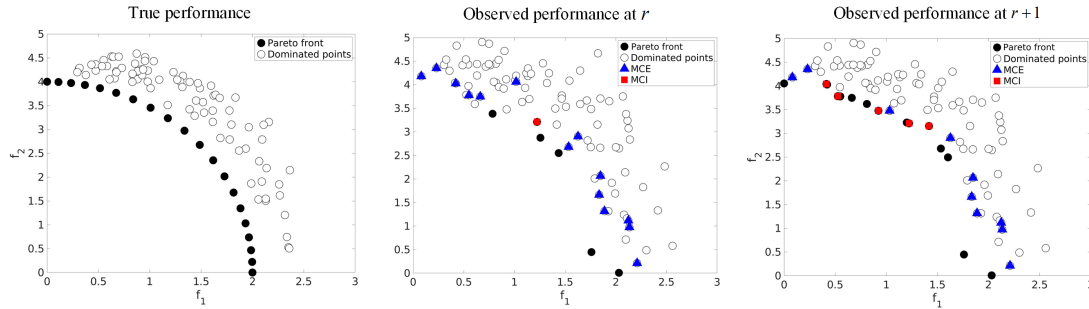


Figure 2: Left panel: True performance of a given set of points. Center panel: Observed performance after r replications. Right panel: Observed performance after $r + 1$ replications.

We thus focus on solving the following (analytically intractable) biobjective problem (see also Lee et al. 2010):

$$\begin{aligned}
 & \min_{r_1, \dots, r_n} a\text{MCE} & \min_{r_1, \dots, r_n} a\text{MCI} \\
 \text{s.t.} & & \text{s.t.} \\
 & \sum_{i=1}^n r_i \leq B & \sum_{i=1}^n r_i \leq B \\
 & r_i \geq 0, i = 1, \dots, n & r_i \geq 0, i = 1, \dots, n
 \end{aligned}$$

where r_i denotes the replications on design i so far, B is the total replication budget, and $a\text{MCE}$ and $a\text{MCI}$ are the approximated misclassification errors. To compute these error approximations, we rely on SK metamodels (Ankenman et al., 2010) to build predictive distributions of the performance of each objective, accounting for the intrinsic noise in the observations, and thus expecting more accurate predictions than the sample means. The relevant background on SK is given in the next section.

4. Stochastic kriging

Let $f(\mathbf{x})$ be an unknown noisy objective function, where $\mathbf{x} = (x_1, \dots, x_d)^T$ is a vector of designs of dimension d . In the interest of fitting a metamodel for the response of this function at n design points, *kriging* or *ordinary kriging* (Sacks et al., 1989; Santner et al., 2013; Kleijnen, 2015), also referred to as *Gaussian Process Regression* (GPR, see e.g., Rasmussen & Williams 2005), is a widely used technique for the subclass of low-dimensional black-box problems. Kriging assumes that the unknown response surface can be represented as $f(\mathbf{x}_i) = \beta + M(\mathbf{x}_i)$, where β is a constant trend and $M(\mathbf{x}_i)$ is a realization of a mean zero covariance-stationary Gaussian random field at the design point \mathbf{x}_i . It is assumed that this field exhibits spatial correlation: i.e., $M(\mathbf{x}_i)$ and $M(\mathbf{x}_k)$ will tend to be

similar when \mathbf{x}_i is close to \mathbf{x}_k in the design space. Essentially, this type of uncertainty is imposed on the problem to aid in developing the metamodel; hence, it is referred to as *extrinsic uncertainty*.

What relates one observation to another is the *covariance function*, denoted k , also referred to as *kernel* or *spatial correlation function*. Multiple covariance functions exist in the field of GPR (see Rasmussen & Williams (2005) for further details); in this work we use the stationary squared exponential, also known as the Gaussian kernel:

$$k_G(\mathbf{x}_i, \mathbf{x}_k) = \sigma^2 \exp \left[- \sum_{q=1}^d \left(\frac{|x_{i,q} - x_{k,q}|}{l_q} \right)^2 \right] \quad (3)$$

with $i, k = 1, \dots, n; i \neq k$ design points, and σ^2, l_q ($q = 1, \dots, d$) are *hyperparameters* that usually need to be estimated, and that denote the process variance, and the length-scale of the process along dimension q , respectively. The hyperparameters are usually unknown, and are commonly estimated using *maximum likelihood estimation* (MLE).

The seminal work of Ankenman et al. (2010) extended the commonly used ordinary kriging model, for representing the response surface implied by a *stochastic* simulation. For a given objective and an arbitrary design point \mathbf{x}_i , the model represents the observed objective value $\tilde{f}_r(\mathbf{x}_i)$ in the r^{th} replication as:

$$\tilde{f}_r(\mathbf{x}_i) = \beta + M(\mathbf{x}_i) + \epsilon_r(\mathbf{x}_i). \quad (4)$$

The first two terms of this equation are equivalent to ordinary kriging. The term $\epsilon_r(\mathbf{x}_i)$ is referred to as *intrinsic uncertainty*, as it is the uncertainty inherent in stochastic simulation (i.e., the noise perturbing the observations). The intrinsic uncertainty is naturally, independent and identically distributed across replications, having mean 0 and variance $\tau^2(\mathbf{x}_i)$ at any arbitrary point \mathbf{x}_i . Note that the model allows for heterogenous noise, implying $\tau^2(\mathbf{x}_i)$ need not be constant throughout the design space. The model also allows for $\text{Corr}[\epsilon_r(\mathbf{x}_i), \epsilon_r(\mathbf{x}_h)] > 0$, as tends to be the case with the use of common random numbers (CRN); yet, this is not desirable, as it inflates the MSE (Eq. 6). This may seem surprising, as discussed in Ankenman et al. (2010), because CRN is used in standard regression models (i.e., models such as $f(\mathbf{x}_i) = \mathbf{f}(\mathbf{x})^T \boldsymbol{\beta} + \epsilon_r(\mathbf{x}_i)$) to reduce the variance of the slope coefficients. However, CRN inflates the variance of the predictor (Eq. 5), because this predictor is a weighted average of the outcomes of already sampled design points. We refer to Ankenman et al. (2010) and Chen et al. (2012) for a detailed discussion and formal results on the impact of CRN on stochastic kriging metamodels.

The **stochastic kriging prediction** $\hat{f}(\mathbf{x}_i)$, and its prediction uncertainty $s^2(\mathbf{x}_i)$ at

any design point \mathbf{x}_i (whether it has been sampled or not) are given by

$$\hat{f}(\mathbf{x}_i) = \beta_0 + \Sigma_M(\mathbf{x}_i, \cdot)^T [\Sigma_M + \Sigma_\epsilon]^{-1} (\bar{\mathbf{f}} - \beta_0 \mathbf{1}_p) \quad (5)$$

$$s^2(\mathbf{x}_i) = \Sigma_M(\mathbf{x}_i, \mathbf{x}_i) - \Sigma_M(\mathbf{x}_i, \cdot)^T [\Sigma_M + \Sigma_\epsilon]^{-1} \Sigma_M(\mathbf{x}_i, \cdot) + \frac{\gamma^T \gamma}{\mathbf{1}_p^T [\Sigma_M + \Sigma_\epsilon]^{-1} \mathbf{1}_p} \quad (6)$$

with $\gamma = 1 - \mathbf{1}_p^T [\Sigma_M + \Sigma_\epsilon]^{-1} \Sigma_M(\mathbf{x}_i, \cdot)$, and Σ_ϵ is the $p \times p$ covariance matrix with (i, h) element

$$\text{cov} \left[\sum_{j=1}^{r_i} \epsilon_j(\mathbf{x}_i)/r^i, \sum_{j=1}^{r_h} \epsilon_j(\mathbf{x}_h)/r^h \right] \quad (7)$$

across all design points \mathbf{x}_h and \mathbf{x}_i ; when CRN are not used, this reduces to the diagonal matrix $\text{diag}[\tau^2(\mathbf{x}_1)/r^1, \dots, \tau^2(\mathbf{x}_p)/r^p]$. The notation $\bar{\mathbf{f}}$ is the vector containing all the observed mean outcomes at the already sampled design points: $\bar{\mathbf{f}} = [\bar{f}(\mathbf{x}_1), \dots, \bar{f}(\mathbf{x}_p)]^T$, with $\bar{f}(\mathbf{x}_i) = \sum_{k=1}^{r_i} \tilde{f}_k(\mathbf{x}_i)/r^i$, and $\mathbf{1}_p$ is a $p \times 1$ vector of ones. Analogous to the ordinary kriging model, Σ_M denotes the $p \times p$ matrix containing the covariances between each couple of already sampled points, as implied by the extrinsic spatial correlation model: $\Sigma_M(\mathbf{x}_i, \mathbf{x}_j) = \text{Cov}[M(\mathbf{x}_i), M(\mathbf{x}_j)]$. The notation $\Sigma_M(\mathbf{x}_i, \cdot)$ is the $p \times 1$ vector containing the covariances between the point under study, and the p already sampled points:

$$\Sigma_M(\mathbf{x}_i, \cdot) = [\text{Cov}[M(\mathbf{x}_i), M(\mathbf{x}_1)], \text{Cov}[M(\mathbf{x}_i), M(\mathbf{x}_2)], \dots, \text{Cov}[M(\mathbf{x}_i), M(\mathbf{x}_p)]]^T. \quad (8)$$

A crucial property of SK that we exploit in this work, is that the SK predictor is not an exact interpolator (as opposed to the ordinary kriging predictor), due to the presence of the intrinsic noise. The details are given in the next section.

5. Proposed MORS procedure

5.1. Proposed sampling criteria

Stochastic kriging uses the performance observed so far (i.e., the sample means and variances), to build the metamodels. Given that SK is not an exact interpolator (see Figure 5), the solutions sampled so far can be re-evaluated using the predictor, to yield a hopefully more accurate approximation of its response (as the predictor accounts for the noise in the observed performance). We are then using both the sample means and variances (denoted \bar{f} and σ^2), respectively the predictor values and uncertainties (denoted \hat{f} and \hat{s}), to allocate replications to those points that are expected to change the current observed Pareto-optimal set the most. The two sampling criteria proposed thus rely on the SK predictions to make decisions, as opposed to relying on the observed means; the observed means and variances are used to guide the allocation procedure. These proposed criteria are referred to as *expected hypervolume difference* (EHVD), and *prior-posterior distance* (PD).

Let S be the entire set of sampled points, PS the *observed* Pareto set of S , and \widehat{PS} the *predicted* Pareto set of S . Then, the evaluation of the points in PS and \widehat{PS} yields the fronts PF and \widehat{PF} , respectively. Furthermore, for a given point \mathbf{x}_i , let $\bar{\mathbf{f}}(\mathbf{x}_i)$ and $\hat{\mathbf{f}}(\mathbf{x}_i)$ be the observed mean objective vectors and predicted objective vectors, respectively. For ease of notation, we use the indices i, k to denote points (also referred to as designs), and \mathbf{f}_{ij} to denote the performance of design i on objective j .

5.1.1. Expected hypervolume difference

The *expected hypervolume change* (EHVC) was proposed in Branke et al. (2016); Branke & Zhang (2019) as a criterion to allocate samples. Analytical expressions were devised for the bi-objective case, with the downside being its high computational complexity (exponential in the number of objectives). As also discussed in Hunter et al. (2019), using the EHVC is more likely to be useful to the decision-maker, as it invests more computational effort in estimating the performance of outstanding points, rather than differentiating between points that are marginally dominated or non-dominated (see Figure 3).

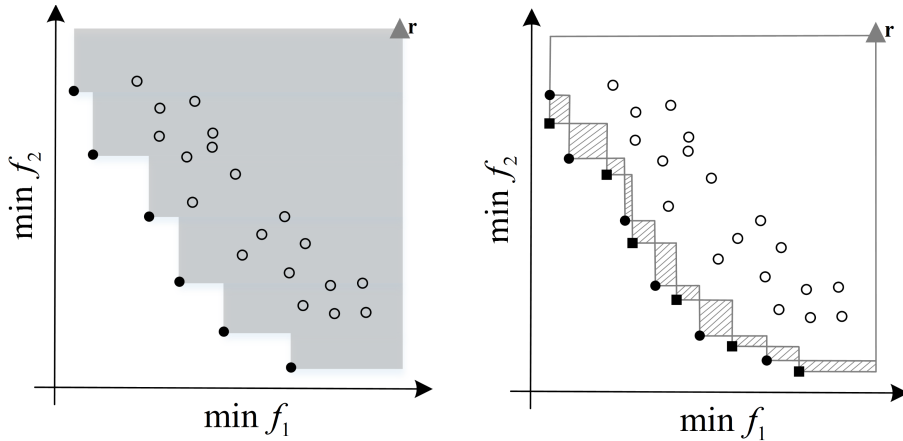


Figure 3: Left panel: Hypervolume (shaded area) dominated by a given non-dominated set (filled points) with respect to a reference point \mathbf{r} . Right panel: the EHVC (shaded area) of a set of non-dominated points with respect to reference point \mathbf{r} . The filled circles denote the current front, and the filled squares the expected change in performance. Empty circles represent the dominated points.

The hypervolume dominated by a given Pareto front A with respect to a reference point \mathbf{r} is defined as the Lebesgue measure, denoted Λ , of the set of objective vectors dominated by the solutions in A , but not by \mathbf{r} :

$$HV(A, \mathbf{r}) = \Lambda \left(\bigcup_{z \in A} \{z \prec z' \prec \mathbf{r}\} \right). \quad (9)$$

Thus, all the non-dominated vectors contribute to the indicator value, and the dominated vectors do not contribute. For two fronts A and B and a reference point \mathbf{r} , the expected

hypervolume change is thus defined as (Branke & Zhang, 2019):

$$EHVC(A, B, \mathbf{r}) := HV(A, \mathbf{r}) + HV(B, \mathbf{r}) - 2 \times \Lambda(HV(A, \mathbf{r}) \cap HV(B, \mathbf{r})). \quad (10)$$

We propose to approximate the EHVC using the SK means to predict how much we expect the HV to change if more samples were allocated to a given point, as we assume the sample mean and predicted mean to coincide when the budget goes to infinity. Thus, for a single point \mathbf{x}_i , the proposed criterion, denoted *expected hypervolume difference* (EHVD), can be calculated as:

$$EHVD^i = |HV(PF) - HV(PF \setminus \bar{\mathbf{f}}(\mathbf{x}_i) \cup \hat{\mathbf{f}}(\mathbf{x}_i))|, \quad \forall i \in S \quad (11)$$

As the computation of the HV only uses the non-dominated points, there are five cases to be considered:

- Case 1: $\bar{\mathbf{f}}(\mathbf{x}_i) \prec \hat{\mathbf{f}}(\mathbf{x}_i)$, and $\bar{\mathbf{f}}(\mathbf{x}_i)$ is on the Pareto front. The HV will change (increase) as the observed vector dominates the predicted vector (see Figure 4(a)).
- Case 2: $\hat{\mathbf{f}}(\mathbf{x}_i) \prec \bar{\mathbf{f}}(\mathbf{x}_i)$, and $\hat{\mathbf{f}}(\mathbf{x}_i)$ is on the Pareto front. The HV will change (decrease) as the predicted vector dominates the observed vector (see Figure 4(b)).
- Case 3: $\bar{\mathbf{f}}(\mathbf{x}_i) \prec \hat{\mathbf{f}}(\mathbf{x}_i)$, $\bar{\mathbf{f}}(\mathbf{x}_i)$ is on the Pareto front, and there are one or more points that dominate $\hat{\mathbf{f}}(\mathbf{x}_i)$ (denoted $\hat{\mathbf{g}}$ in Figure 4(c)). The HV will change (increase) as the sample vector dominates the predicted vector, but the change is not equally significant as in case (a).
- Case 4: $\hat{\mathbf{f}}(\mathbf{x}_i) \prec \bar{\mathbf{f}}(\mathbf{x}_i)$, $\hat{\mathbf{f}}(\mathbf{x}_i)$ is on the Pareto front, and there are one or more points that dominate $\bar{\mathbf{f}}(\mathbf{x}_i)$ (denoted $\hat{\mathbf{g}}$ in Figure 4(d)). The HV will change (decrease) as the predicted vector dominates the sample vector, but the change is not equally significant as in case (b).
- Case 5: $\bar{\mathbf{f}}(\mathbf{x}_i) \prec \hat{\mathbf{f}}(\mathbf{x}_i)$ or viceversa, and both performance vectors are observed in the dominated space. The HV will thus not change and will not impact the EHVD (see Figure 4(e)).

Clearly, the EHVD will be biased to allocate replications on points belonging to cases 1 and 2; points belonging to cases 3-4 may have little or no replications allocated, while points in case 5 will not be considered, though they may as well belong to the true non-dominated set. This is true especially when the noise is high and/or strongly heterogeneous, and thus the sample and predicted means are both relatively far from the true performance; indeed, an extra replication on a given point might then significantly change its position in the objective space.

5.1.2. Posterior distance

To overcome the aforementioned limitations of the EHVD, we propose to additionally use the Euclidean distance between the sample means and the predicted means (i.e., the posterior means). We thus refer to this criterion as the *prior-posterior distance*, denoted

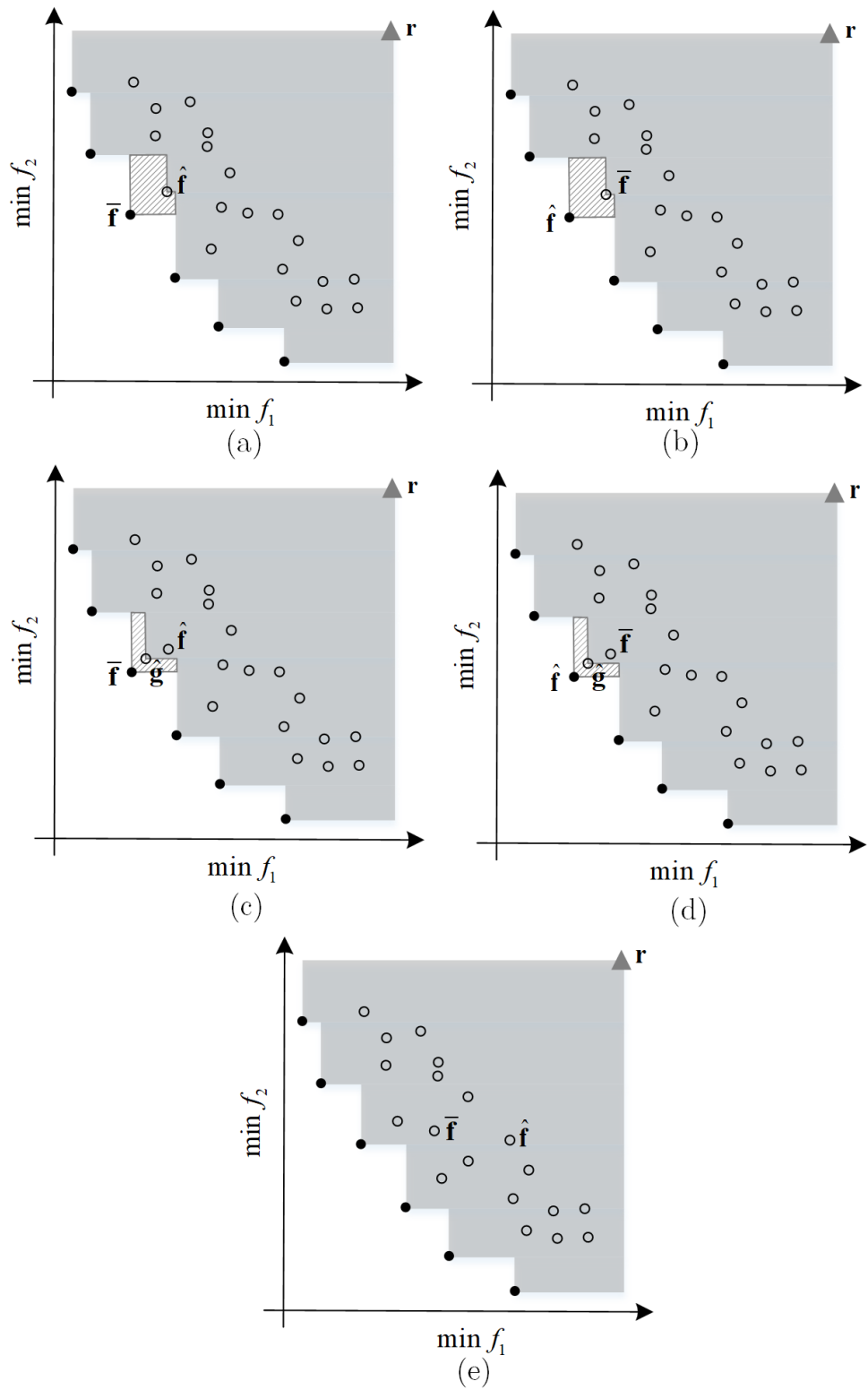


Figure 4: The five cases to be considered when calculating the EHVD.

PD. If the sample mean and prediction are far away from each other, by running more replications on these points, we expect them to come closer to each other and move towards the true position of the point in the objective space, which aids in minimizing both MCE

and MCI errors.

Instead of using the predictions directly, we opt for using the *farthest* confidence bound of $\hat{f}_j(\mathbf{x}_i)$ with respect to $\bar{f}_j(\mathbf{x}_i)$ for objective j . The choice of the farthest confidence bound is because we intend to inflate the PD when the uncertainty of the predictor is high, such that points with high uncertainty will be rewarded more (see Figure 5 for an illustration). We then define the PD between the observed and predicted means as:

$$\text{PD}_i = \sqrt{\sum_{j=1}^m \left[\left| \bar{f}_j(\mathbf{x}_i) - \hat{f}_j(\mathbf{x}_i) \right| + \hat{s}_j^i \right]^2}, \quad \forall i \in S. \quad (12)$$

The farthest confidence bound of the predicted values for each objective is analogous to the *lower confidence bound* (\widehat{LCB}) of the non-dominated points, or the *upper confidence bound* (\widehat{UCB}) of the dominated points (based on the predicted means). These bounds are commonly used in kriging-based optimization as a way to take into account the predictor uncertainty during the search for solutions (Ponweiser et al., 2008; Emmerich et al., 2006), as they minimize the exclusion of potential promising solutions at the cost of a higher number of evaluations. The \widehat{LCB} and \widehat{UCB} are defined as

$$\hat{f}_j(\mathbf{x}) \pm \omega \hat{s}_j(\mathbf{x}), j = 1, \dots, m \quad (13)$$

where ω is usually an integer in the interval $[1, 3]$, yielding the 68%, 95% and 99% confidence intervals (CI) of the prediction respectively (Rasmussen & Williams, 2005). Clearly, in Eq. 12, $\omega = 1$. Analogously, the CI of the observed means (denoted LCB and UCB) are defined as $\bar{f}_j(\mathbf{x}) \pm \omega \sigma(\mathbf{x}), j = 1, \dots, m$. Later in Section 5.2, both the upper and lower confidence bounds for both the sample means and predicted means will be used in the proposed screening procedures.

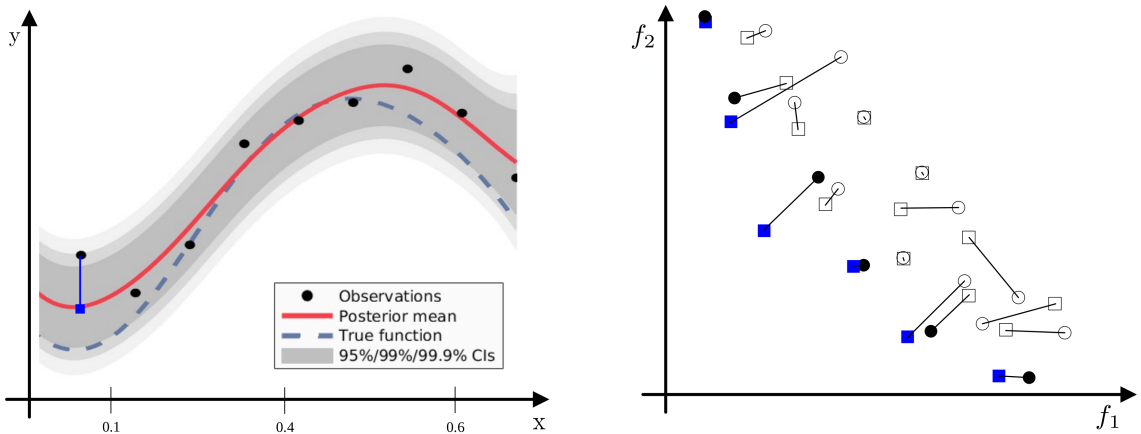


Figure 5: Left panel: Sample means (black dots), SK predictions (red line) and prediction uncertainty (gray area) for a single objective. The distance between the prediction and the sample mean is denoted with a blue line. Right panel: The posterior distance between the sample means (circles) and predicted means (squares). The observed and predicted fronts are depicted with filled circles and squares respectively.

5.1.3. Algorithm outline

For ease of reference, the different sets of points used in the proposed algorithms are summarized in Table 1; the steps of the proposed MORS procedure are stated in Algorithm 1:

Table 1: Overview of the different sets of points used in the proposed algorithms.

Notation	Description
S	Entire set of sampled points.
PS	Pareto set based on sample means.
PF	Pareto front based on sample means.
\widehat{PS}	Pareto set based on predicted means.
\widehat{PF}	Pareto front based on predicted means.
UCB	Set of the upper confidence bounds of all points in PS .
\widehat{UCB}	Set of the upper confidence bounds of all points in \widehat{PS} .
LCB	Set of the lower confidence bounds of all points in $S \setminus PS$.
\widehat{LCB}	Set of the lower confidence bounds of all points in $S \setminus \widehat{PS}$.

At the initial step the algorithm fits a stochastic kriging metamodel to each objective, based on the observed mean objective values and respective variances of the sampled points in S . The metamodels are then used to approximate each response on these sampled points. The current observed Pareto-optimal sets are obtained based on both the observed means (PS and PF) and predicted means (\widehat{PS} and \widehat{PF}). In the next step, the upper and lower confidence bounds for each point are calculated. Using these confidence bounds, if a screening procedure is invoked (lines 11-13 in Algorithm 1), the algorithm filters out from the *current* iteration the points that are observed as clearly inferior. Note that these points might be considered in further iterations. We propose two screening procedures, described in the following section, that will use both the observed and predicted Pareto fronts.

The algorithm proceeds to calculate the EHVD values using Equations (9) and (11), and the PD values using Equation (12). Each of these are then normalized in the $[0, 1]$ interval, as it is possible to have very high values of EHVD relative to PD. Consequently, the criterion used to rank and select points in the current iteration will be given by the Pareto front between the maximization of both criteria (see Figure 6), as they reward different components: while the EHVD is biased to allocate budget to those points that are expected to change the current HV the most, the PD focuses on reducing the uncertainty on points with competitive performance (note that the number of points in this Pareto front can differ per iteration). As it will be shown in the experimental results, the non-dominated set of this trade-off outperforms the individual performance of each proposed criterion.

Algorithm 1 SK-MORS algorithm

- 1: **Input:**
 - 2: S ▷ Set of sampled points
 - 3: b ▷ Initial number of replications per design point
 - 4: $B = |S| \times b$ ▷ Replications to be allocated per iteration
 - 5: **Output:**
 - 6: PS ▷ The observed Pareto set
 - 7: **while** stopping criterion not met **do**
 - 8: Fit a SK metamodel to each objective j : $\hat{f}_j(\mathbf{x})$
 - 9: Compute UCB , LCB , \widehat{UCB} and \widehat{LCB}
 - 10: **procedure** SCREENING(UCB , LCB , \widehat{UCB} , \widehat{LCB})
 - 11: $\tilde{S} \leftarrow$ Set of points screened out based on sample means
 - 12: $\hat{S} \leftarrow$ Set of points screened out based on predicted means
 - 13: $\tilde{S} = S \setminus (\tilde{S} \cap \hat{S})$ ▷ Temporarily remove clearly inferior points
 - 14: **end procedure**
 - 15: Compute and normalize the $EHVD_i$ and PD_i values, $\forall i \in \tilde{S}$
 - 16: $\widetilde{PF} \leftarrow$ Pareto front of \tilde{S} maximizing both PD and EHVD
 - 17: $T_i = \frac{B}{|\widetilde{PF}|}$, $\forall i \in \widetilde{PF}$
 - 18: Allocate T_i replications to each i in \widetilde{PF}
 - 19: **end while**
 - 20: Return the PS .
-

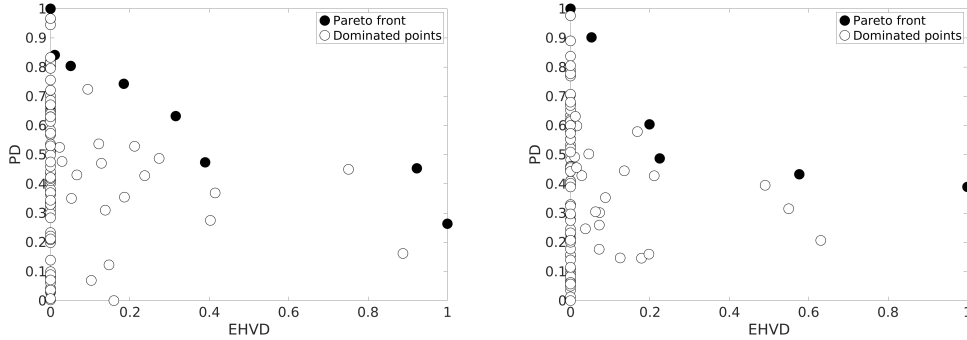


Figure 6: Pareto front between the maximization of both criteria at two arbitrary iterations.

In the final steps, the allocation quantity is determined based on the total budget available per iteration (using general rounding rules). The input parameter b determines how many replications could be performed per design point if these were distributed equally. Thus, the total number of replications B to be allocated per iteration, depends on the initial number of candidate points in S . As the algorithm will not allocate replications equally, a significantly higher number of replications $T_i \gg b$ will be allocated to the selected points in \widetilde{PF} . If the stopping criterion is met, the algorithm returns the observed Pareto set. As the proposed allocation procedure is sequential, after the budget in the current iteration has been depleted, the SK parameters are recomputed with the new (more accurate) observed means and variances to perform a new iteration.

5.2. Screening procedures

As is well-known in ranking and selection, in many cases some of the points included in the solution set will be clearly inferior to other solutions in the set (Boesel et al., 2003). *Screening* or *subset-selection* heuristics are widely used prior to running the ranking and selection procedure in order to filter out these clearly inferior solutions. We propose two subset selection procedures that will exploit both the sample variance and prediction uncertainties to enclose confidence regions that reduce the number of points to be considered at each iteration. Unless stated otherwise, hereafter we will use a value of $\omega = 3$ for Eq. 13, in order to enclose the 99% CI.

The first of the proposed screening procedures is outlined in Algorithm 2. The worst confidence bounds among all the non-dominated points for each objective j , denoted \bar{u}_j for the observed means, and \hat{u}_j for the predicted means, are used to enclose a confidence region (see left panel of Figure 7). The second screening procedure, outlined in Algorithm 3, will instead enclose a confidence region using the upper confidence bounds of *all* the non-dominated points (see right panel of Figure 7). These confidence regions are computed for *both* the PF and \widehat{PF} .

Algorithm 2 SCREENING BOX

```

1: Input:  $UCB, LCB, \widehat{UCB}$  and  $\widehat{LCB}$ 
2:  $\bar{S} = \emptyset$  ▷ Initialize set of clearly inferior points
3:  $\bar{u}_j: \max_{i \in PF} UCB_{i,j}, j = 1, \dots, m$ 
4:  $\hat{u}_j: \max_{i \in \widehat{PF}} \widehat{UCB}_{i,j}, j = 1, \dots, m$ 
5:  $NP = S \setminus PS \cap S \setminus \widehat{PS}$ .
6: for  $i \in NP$  do
7:   for  $j = 1 : m$  do
8:     if  $LCB_{ij} > \bar{u}_j$  &&  $\widehat{LCB}_{ij} > \hat{u}_j$  then
9:        $\bar{S} \cup \{\mathbf{x}_i\}$ 
10:      break
11:    end if
12:  end for
13: end for
14: return  $\bar{S}$ 

```

Subsequently, the performance of every dominated point (denoted with empty circles) is substituted by the lower confidence bounds (denoted with empty squares). Similarly, the performance of the non-dominated points (denoted with filled circles) is substituted by the upper confidence bounds (denoted with filled squares). This is done for both, the performance based on sample means and the performance based on predicted means. If the new position of a given dominated point does not enter any of the confidence regions enclosed by the non-dominated points (i.e., the region enclosed by PF or \widehat{PF}), then this point is screened out from the *current* iteration (see e.g., points a and b in Figure 7). Otherwise, it will be considered in the current iteration (see e.g., points c and d in Figure 7). This is to ensure that, even with very high noise levels (as in the experiments in Section

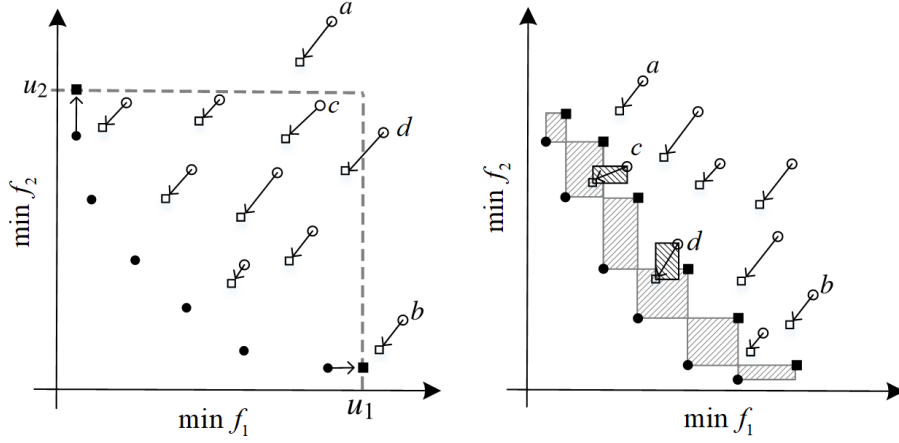


Figure 7: Illustration of both screening procedures proposed: SCREENING BOX (left panel) and SCREENING BAND (right panel). Filled marks denote the non-dominated points, and unfilled marks the dominated points. The performance is denoted with circles, and confidence bounds with squares.

Algorithm 3 SCREENING BAND

```

1: Input:  $UCB, LCB, \widehat{UCB}$  and  $\widehat{LCB}$ 
2:  $\bar{S} = \emptyset$  ▷ Initialize set of clearly inferior points
3:  $NP = S \setminus PS \cap S \setminus \widehat{PS}$ 
4: procedure DISTANCE( $\mathbf{f}_i, \mathbf{f}_k$ )
5:    $h_{ik} = \sqrt{\sum_{j=1}^m [f_{ij} - f_{kj}]^2}$ 
6:   return  $h_{ik}$ 
7: end procedure
8: for  $i \in NP$  do
9:    $\bar{h}_{ik} = \text{DISTANCE}(LCB_i, UCB_k), \forall k \in PF$ 
10:   $\hat{h}_{ik} = \text{DISTANCE}(\widehat{LCB}_i, \widehat{UCB}_k), \forall k \in \widehat{PF}$ 
11: end for
12: for  $i \in NP$  do
13:   $u = \min_{k \in PF} \bar{h}_{ik}$ 
14:   $v = \min_{k \in \widehat{PF}} \hat{h}_{ik}$ 
15:  for  $j = 1 : m$  do
16:    if  $LCB_{ij} > UCB_{uj}$  &&  $\widehat{LCB}_{ij} > \widehat{UCB}_{vj}$  then
17:       $\bar{S} \cup \{\mathbf{x}_i\}$ 
18:      break
19:    end if
20:  end for
21: end for
22: return  $\bar{S}$ 

```

6.1), with a high confidence we are not excluding truly non-dominated solutions.

6. Numerical experiments

The experiments are designed to (1) evaluate the performance of the two proposed resampling criteria against EQUAL allocation (which uniformly distributes the replication budget) and the state-of-the-art MOCBA algorithm, (2) test the impact of the two

screening procedures proposed, and (3) examine the impact of using the SK information instead of the sample means and variances. We present the results for 2 objectives with varying number of decision variables, with low, medium and high levels of noise, on a set of artificial test problems with different Pareto front geometries. Extending the algorithm to more objectives is straightforward, as we can build metamodels for as many objectives as it is necessary; however, the computational cost will significantly increase due to the double hypervolume computations in Equation 11, and the identification problem also increases in complexity for higher-dimensional objective spaces (Cooper & Hunter, 2020). We thus leave the analysis for 3 and more objectives for further work.

We opt for stopping the algorithms after a fixed number of samples have been allocated; this is a realistic criterion, as in practice, it is not possible to determine whether the algorithm has correctly identified the entire true Pareto set at a given iteration (i.e., when there are no zero misclassification errors). The (fixed) budget per macroreplication (i.e., per full algorithm run) depends on the budget per iteration B , the size of the candidate set S being considered, and the initial number of replications per point b . Table 2 summarizes the parameters for the experiments.

Table 2: Summary of the experimental parameters

Kriging metamodels	
Kernel: Gaussian	$k_G(\mathbf{x}, \mathbf{x}') = \sigma^2 \exp \left[- \sum_{i=1}^m \left(\frac{ \mathbf{x}_i - \mathbf{x}'_i }{\sqrt{2}l_i} \right)^2 \right]$
Noise levels	
Low noise	$0.001 \times R_f^j \leq \tau(\mathbf{x}) \leq 0.5 \times R_f^j$
Medium noise	$0.01 \times R_f^j \leq \tau(\mathbf{x}) \leq 1 \times R_f^j$
High noise	$1 \times R_f^j \leq \tau(\mathbf{x}) \leq 2 \times R_f^j$
Replication budget per iteration	
$B = S \times b$	

To assess the performance of the proposed procedures, we use the WFG3, WFG4 and DTLZ7 functions (Huband et al., 2006). The WFG test suite is a state-of-the-art scalable test problem toolkit, which allows to construct problems with any number of objectives and decision variables; features such as modality and separability can be customized, using a set of shape and transformation functions. WFG3 is a non-separable and unimodal problem with a linear and degenerate Pareto front, WFG4 is a separable and multimodal problem with a concave geometry of the Pareto front, and DTLZ7 is a disconnected and multi-modal problem with mixed parameters (see Huband et al. (2006) for the analytical expressions and detailed characteristics of these functions). The set of points S being considered (which we also refer to as the decision space) is discrete and contains a fixed and known number of truly Pareto optimal points, denoted PS_t . Table 3 summarizes the experimental scenarios, and Figure 8 illustrates the objective space of the test functions.

Table 3: Summary of the experimental scenarios

	WFG3	WFG4	DTLZ7
Number of objectives m	2	2	2
Number of decision variables d	5	5	2
Number of sampled points $ S $	100	100	100
Size of the true Pareto set $ PS_t $	20	20	50
Noise level	High	Medium	Low
Total replication budget per iteration B	500	500	500
Total number of iterations	15	30	30

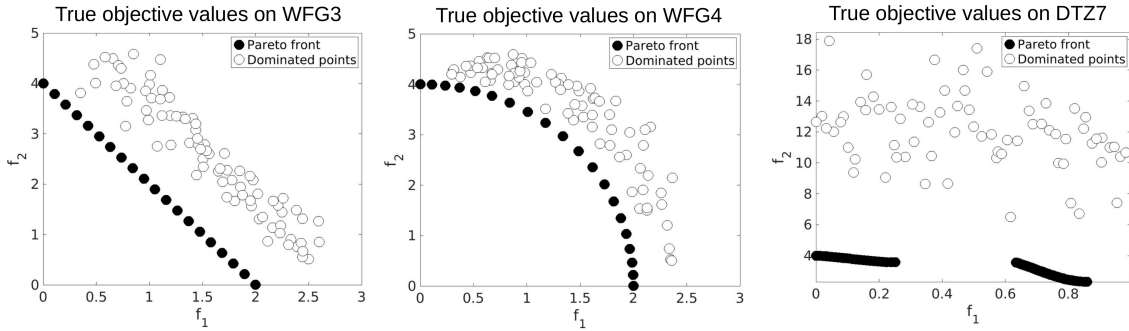


Figure 8: True Pareto front (PF_t , black points) and dominated points in the bi-objective scenarios.

The true objective outcomes are perturbed with heterogeneous Gaussian noise. Hence, we obtain noisy observations $\tilde{f}_r^j(\mathbf{x}^i) = f^j(\mathbf{x}^i) + \epsilon_r(\mathbf{x}^i)$, with $\epsilon_r(\mathbf{x}^i) \sim \mathcal{N}(0, \tau(\mathbf{x}^i))$ for $j = 1, \dots, m$ objectives at the r^{th} replication. In practice, the noise can follow any type of structure. In our experiments, we assume that the standard deviation of the noise, $\tau(\mathbf{x})$, varies linearly with respect to the objective values, as is common in the literature (Picheny et al., 2013; Jalali et al., 2017; Rojas-Gonzalez et al., 2020). The maximum and minimum values of $\tau(\mathbf{x})$ are linked to the range of each objective value in the region of interest (i.e., $R_f^j = \max_{\mathbf{x} \in S} f^j(\mathbf{x}) - \min_{\mathbf{x} \in S} f^j(\mathbf{x}), j = 1, \dots, m$). As shown in Table 2, we consider three levels of noise perturbing the responses (low, medium and high), varying between $0.001R_f^j$ and $2R_f^j$. The three analytical test functions also vary in difficulty; WFG3 is easier to solve than WFG4, and the latter is easier than DTLZ7. This is due to the shape and geometry of the front, and the domain and range of the functions. Moreover, we consider the case where the noise decreases linearly with the objective values, yielding minimum noise at the global minimum of each individual objective. To quantitatively evaluate the performance of the algorithms, we use the F1 metric (14) as a measure to evaluate the accuracy of the Pareto set identified by the algorithms (see, e.g., Fawcett 2006; Ting 2017; Powers 2020 for further details on the F1 metric):

$$F1 = 2 \left(\frac{\text{precision} \times \text{recall}}{\text{precision} + \text{recall}} \right) \quad (14)$$

where

$$precision = \frac{\text{true positives}}{\text{true positives} + \text{false positives}} \quad (15)$$

and

$$recall = \frac{\text{true positives}}{\text{true positives} + \text{false negatives}}. \quad (16)$$

Note that Equations 15 and 16 are analogous to the MCI and MCE errors respectively; thus, the F1 metric takes a value between zero and one and weighs both misclassification errors equally: if the algorithm correctly identifies the entire PS_t and does not misclassify any truly dominated points, then $F1 = 1$.

6.1. Results

We first evaluate the performance of the proposed SK-MORS algorithm with the default screening procedure (i.e., using the SCREENING BOX procedure), referred to as SKMORS1, against EQUAL allocation (i.e., b replications are allocated to every point in S at each iteration) and the MOCBA algorithm (see Appendix A for the allocation rules), which we consider state-of-the-art. In EQUAL and MOCBA, the *observed means* are used instead of the SK predictions. To analyze the benefit of using the SK information instead of the observed means, we also compare SKMORS against versions of the EQUAL allocation and MOCBA algorithms that use stochastic kriging predictions instead of the observed means to *identify* the non-dominated points (denoted EQUAL-SKi and MOCBA-SKi respectively). In addition, we evaluate a version of MOCBA which uses the SK information also to compute the allocation rules (i.e., using the predicted means and MSE instead of sample mean and variance; this is referred to as MOCBA-SK). We also evaluate the impact of the proposed SCREENING BAND procedure in the algorithm (which we refer to as SKMORS2), and a version that doesn't use any screening (referred to as SKMORS0). Furthermore, the impact of the proposed sampling criteria is analyzed by comparing the performance of an algorithm using only the EHVD criterion (denoted SKMORS-HV), and using only the PD criterion (denoted SKMORS-PD). In all cases, we run the algorithms 30 times on the same instance (i.e., 30 macrorreplications); in the figures, we report the average F1 value obtained at each iteration of the algorithms, along with the 95% confidence intervals. Table 4 summarizes the algorithms evaluated, and Figure 9 shows the evolution of the F1 metric in terms of the number of iterations performed, . Figure 10 evaluates the different components of the proposed algorithm for WFG4 (analogous results were observed on the other test problems).

It is clear from the plots in Figure 9, that the speed of convergence of EQUAL and MOCBA allocation rules towards the correct identification of the true Pareto front is drastically outperformed by the proposed algorithm, for all test problems considered. The convergence rate observed in scenario WFG4 (Figure 9(b)), where MOCBA outperforms EQUAL, is expected. However, this is not observed in Figures 9(a) and 9(c), as in these scenarios a much larger budget is required for convergence of MOCBA and EQUAL; the proposed method on the other hand, shows consistent performance. Moreover, from

Table 4: Overview of the different algorithms tested.

Algorithm	Description
SKMORS-0	SK-MORS algorithm without using a screening heuristic.
SKMORS-1	SK-MORS algorithm using the SCREENING BOX heuristic (Algorithm 2).
SKMORS-2	SK-MORS algorithm using the SCREENING BAND heuristic (Algorithm 3).
SKMORS-PD	SK-MORS algorithm using only the PD criterion.
SKMORS-HV	SK-MORS algorithm using only the EHVD criterion.
EQUAL	Allocate replications uniformly to all sampled points.
EQUAL-SKi	EQUAL allocation using the SK predictions for identification.
MOCBA	Multiobjective Optimal Computing Budget Allocation algorithm.
MOCBA-SK	MOCBA algorithm using the SK predictions for allocation and identification.
MOCBA-SKi	MOCBA algorithm using the SK predictions only for identification.

scenario WFG3 and WFG4, we can observe that not only the rate of convergence but also the reduction of variability rates are faster. It is also remarkable that in scenario WFG4 the SK predictions provide much superior estimates already from the beginning of the procedure, which we attribute to the low level noise compared to the other scenarios.

The positive impact of the proposed screening procedures is shown in Figures 10(a) and 10(b); the metric $|S|$ conveys the number of points to be considered at a given iteration. Both screening procedures succeed in sequentially reducing the number of candidate points considered as the observed performance becomes more accurate; evidently, the biggest reduction is obtained with SCREENING BAND. Such reduction significantly benefits the proposed method, as the computational cost of executing the hypervolume calculations in Eq. 11 (for every candidate point, at each iteration) grows exponentially with the number of objectives. Moreover, the use of the screening procedures does not impact the performance of the proposed algorithm w.r.t. the convergence to the true front.

As the scenarios tested are quite extreme in terms of noise levels, filtering out some points may result in leaving out a truly non-dominated point in one or more iterations (i.e., MCE points), especially for the SCREENING BAND procedure as it uses a narrower confidence region. Overall, no particular differences are observed between both proposed methods, except for the fact that SCREENING BAND has a higher risk of filtering out true non-dominated points. Thus, for practical purposes, both screening procedures proposed provide a reliable confidence region to filter out clearly inferior points and reduce the computational burden.

Figure 10(c) shows that the convergence to be more slightly more effective for SKMORS1 (i.e., using the trade-off between both resampling criteria, see Figure 6), than using the PD and EHVD separately. Overall, the performance of both resampling criteria are observed to be competitive, but bring greater benefit when they are combined. We confirmed this observation in further experiments with increasing levels of noise, where the use of both criteria separately becomes increasingly inferior. This is expected, given that one criterion complements the limitations of the other: while the EHVD rewards more those

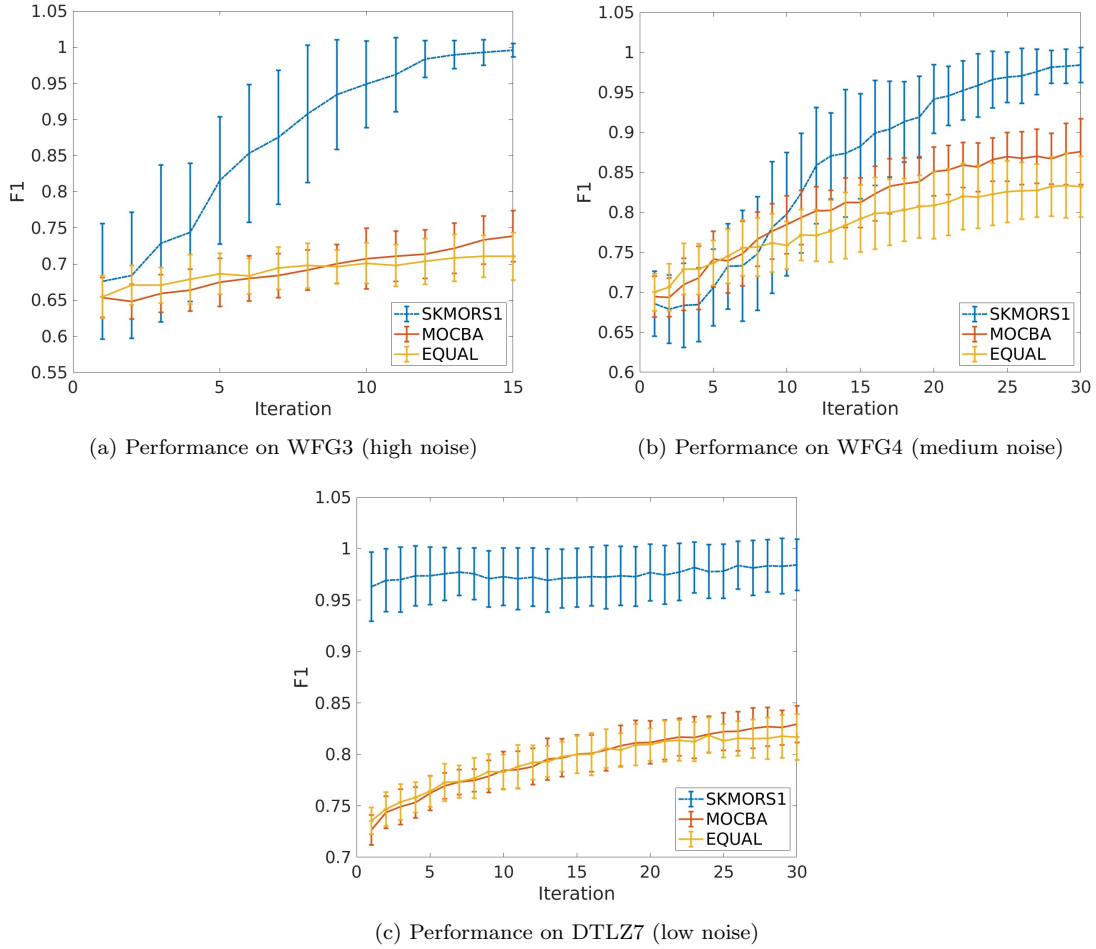


Figure 9: Convergence to the true Pareto front: the proposed algorithm versus standard EQUAL allocation, and the state-of-the-art MOCBA procedure, for the 3 test problems considered.

points in cases 1 and 2 discussed in Section 5.1.1, the PD rewards more those points with high uncertainty and does not care about domination, only about improving the location (performance) of the points closer to the true location. An advantage of the PD criterion over the EHVD criterion is its low computational cost.

Finally, the identification of the points with the true best expected performance is largely facilitated by exploiting the stochastic kriging information (as opposed to relying on the observed means); as evident from Figure 10d, EQUAL-SKi and MOCBA-SKi drastically outperform EQUAL and MOCBA, yet still show worse performance than SKMORS1. The bad performance of MOCBA-SK is remarkable; this however, is not entirely surprising: MOCBA is formulated on the premise that the observed sample mean and variance for a given design follow a normal distribution (see Equation 1), and the stochastic kriging MSE does not reflect this variability, only the correlation strength between the design point and the response to be predicted.

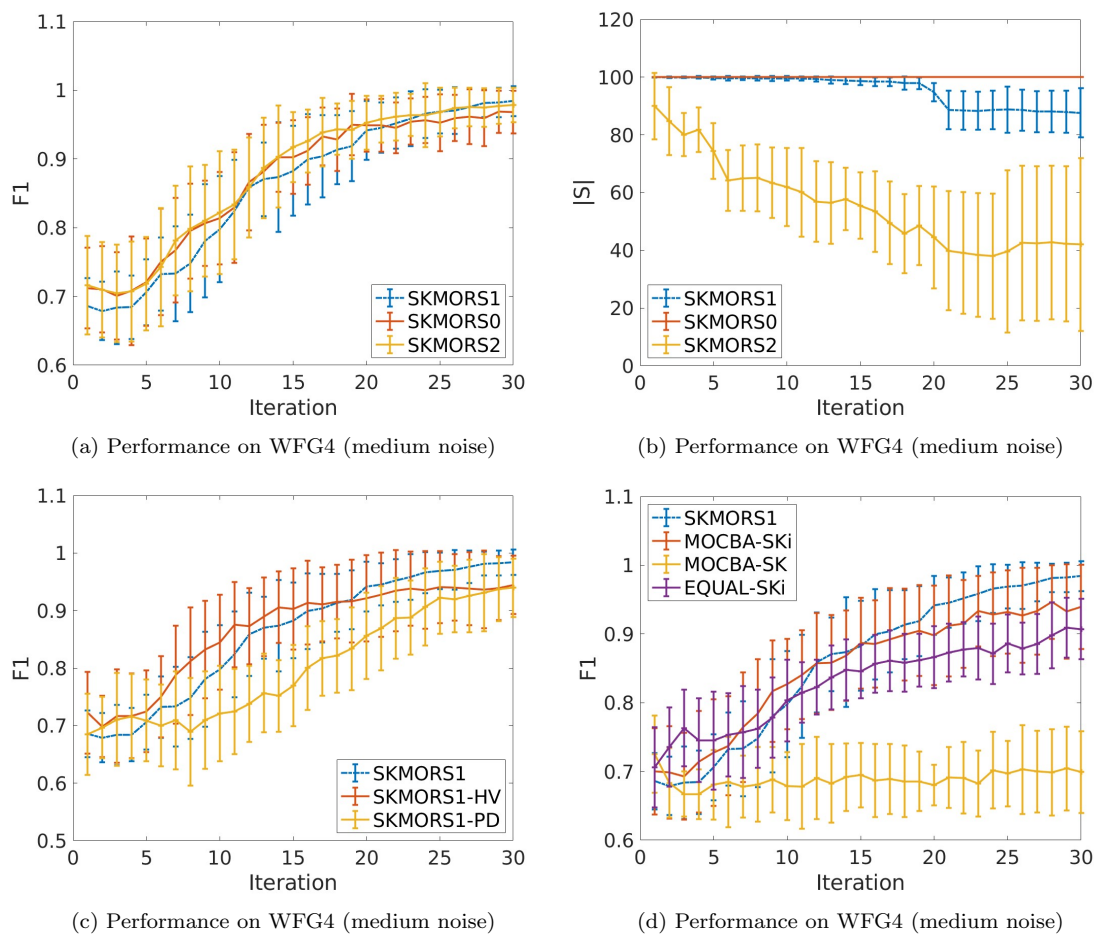


Figure 10: Performance of the of the different components of the proposed algorithm.

6.2. Performance with standard metrics for deterministic multiobjective optimization

In this work we opted for the F1 performance metric as we believe it provides a reliable way to evaluate algorithmic performance in the MORS context, as it measures the progress in decision space (as opposed to the uncertain performance in output space). Even though we use hypervolume in a method to allocate samples, as the hypervolume contributions are indeed useful in MORS, it's worth stressing that standard performance metrics for (deterministic) multiobjective optimizers (Li & Yao, 2019), such as *hypervolume* or the *inverted generational distance* (i.e., the average distance to the closest member of the true Pareto front), are ill-suited for the evaluation of stochastic multiobjective optimizers (Binois et al., 2015; Rojas-Gonzalez et al., 2020), due to the noise in the observed performance. For instance, in deterministic settings, a higher value of hypervolume means a better quality of the Pareto set (i.e., it is Pareto-compliant); however, in the stochastic case, the noisy performance may increase or decrease the true hypervolume values and thus, it would be misleading to compare algorithms in our setting using these metrics. The quantitative performance evaluation of stochastic Pareto fronts is a field still in its infancy, offering significant opportunities for further work (see our comments in Section 7). Figure 11 below provides an example of this crucial issue; HV_{gap} is the absolute value

of the difference between the true hypervolume and the observed hypervolume, as this difference can be negative or positive: $HV_{\text{gap}} = |\text{TrueHV} - \text{ObsVH}|$.

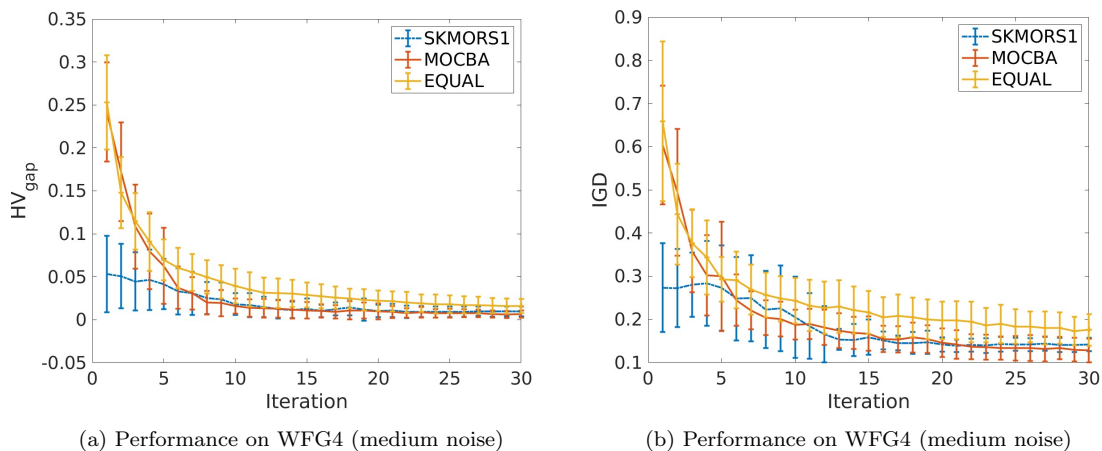


Figure 11: Performance evaluation using standard metrics for deterministic multiobjective optimizers. The predicted means (SKMORS1) and sample means (MOCBA and EQUAL) are used to compute these indicators.

Relying on the performance based on hypervolume and IGD, would clearly lead to incorrect inference about the overall performance of the algorithms, as by comparing with Figure 9 (b), it is clear that the real performance of the proposed algorithm is superior to MOCBA, and this one in turn is superior to EQUAL. Moreover, we observed quasi-identical behaviour in the experiments with scenarios WFG3 and DTLZ7. Using these metrics, the performance is observed very similar between the algorithms, because the decision spaces are designed such that all the points are close to the true front (see Figure 8), for it to be difficult for the algorithms to converge to zero errors when perturbed by noise.

7. Conclusions and future research

We have proposed a multiobjective ranking and selection technique that can deal with heteroscedastic noise and exploit correlations between the alternatives by using stochastic kriging metamodels. By means of two novel sampling criteria, we are able to allocate samples efficiently in view of reducing both misclassification errors. We have extended previous work which has proposed the hypervolume as a good criterion to allocate samples; however, computing the expected hypervolume change exactly is computationally expensive. We have thus proposed an approximation (Expected Hypervolume Difference) that uses the stochastic kriging posterior means as reliable predictive distributions of the noisy objectives. Additionally, we proposed a complementary measure (Posterior Distance) that simply looks at the distance between the observed sample means and the stochastic kriging posterior means (and the MSE of the prediction), as a criterion to allocate samples. Both criteria showed competitive performance individually, but best results were obtained when combined.

The EHVD on one hand focuses on points that have high probability of changing the current hypervolume, which means the hypervolume may increase or decrease, but arguably the points selected by the EHVD are interesting for the decision-maker. However, due to the noise perturbing the objectives, we found that this criterion on its own ignores some alternatives that may be truly non-dominated, as only the *observed* non-dominated set is used to compute the hypervolumes. The PD on the other hand, focuses on improving the position accuracy of all the alternatives in objective space, and explicitly neglects the dominance relationships between the alternatives. The PD has the additional advantage of being significantly cheaper to compute. By sampling on the Pareto front depicted by the maximization of both criteria, we are able to efficiently allocate crucial computational budget to a very sensible and thus informative subset of alternatives.

To aid in reducing the number of alternatives at each iteration, we proposed two screening procedures that exclude inferior alternatives at each iteration by building a confidence region around the observed and predicted Pareto fronts. Note that unlike in the single objective case, the dominance relationships may change radically after one iteration, and thus all alternatives must be considered at the start of each iteration. Both screening procedures proposed showed competitive and comparable performance, with the key difference that SCREENING BOX is more risk-averse in terms of the number of points considered at each iteration. The choice of which one to use will depend on the specific problem at hand (e.g., noise levels).

Our results have highlighted that the use of standard performance metrics for multi-objective optimization, such as hypervolume and IGD, can be very misleading in noisy settings, especially in settings with input-dependent noise. As we tested the algorithms on known analytical functions perturbed by artificial noise, we could reliably evaluate the performance in the input space (and thus the choice of the F1 metric). Obviously, this is not possible in practice, where the true Pareto set is unknown. The current literature does not offer metrics to reliably assess the performance of stochastic multiobjective optimizers, which we consider a crucial challenge for further work. Finally, even though the method is straightforwardly scalable to more objectives, higher-dimensional objective spaces pose a challenge the MORS research, as the discrete set to approximate the non-dominated front grows exponentially with the number of objectives, and thus the computational cost increases significantly; we thus believe that a thorough study with more objectives is non-trivial and poses a major challenge to the MORS community as well.

Appendix A MOCBA allocation rules

The allocation rules for the simplified MOCBA algorithm Chen & Lee (2010) are summarized below:

\bar{f}_{ij} : The averaged observed performance of design i for objective j after a certain number of replications.

p_i : The design that dominates design i with the highest probability.

$j_{p_i}^i$: The objective j of p_i that dominates the corresponding objective of design i with the lowest probability.

τ_{ij} : The observed intrinsic variance of design i for objective j after a certain number of replications.

α_i : The budget allocation for design i .

S : The entire set of sampled points.

S_A : The subset of designs in S labeled as being dominated.

S_B : The subset of designs in S labeled as being non-dominated.

For any given design $g, h \in S_A$ and $d \in S^B$:

$$\alpha_h = \left(\frac{\tau_{hj_{p_h}}^2 / \delta_{hp_h j_{p_h}}}{\tau_{gj_{p_g}}^2 / \delta_{gp_g j_{p_g}}} \right)^2 \quad (17)$$

$$\alpha_d = \sqrt{\sum_{h \in D_d} \frac{\tau_{dj_d}^2}{\tau_{hj_d}^2} \alpha_h^2} \quad (18)$$

where

$$\delta_{ipj} = \bar{f}_{ij} - \bar{f}_{pj} \quad (19)$$

$$j_p^i = \arg \min_{j \in \{1, \dots, m\}} P(\bar{X}_{pj} \leq \bar{X}_{ij}) = \arg \max_{j \in \{1, \dots, m\}} \frac{\delta_{ipj} |\delta_{ipj}|}{\tau_{ij}^2 + \tau_{pj}^2} \quad (20)$$

$$p_i = \arg \max_{\substack{p \in S \\ p \neq i}} \prod_{j=1}^m P(\bar{f}_{pj} \leq \bar{f}_{ij}) = \arg \min_{\substack{p \in S \\ p \neq i}} \frac{\delta_{ipj_p^i} |\delta_{ipj_p^i}|}{\tau_{ij_p^i}^2 + \tau_{pj_p^i}^2} \quad (21)$$

$$S_A = \left\{ h | h \in S, \frac{\delta_{hp_h j_{p_h}}^2}{\tau_{hj_{p_h}}^2 + \tau_{p_h j_{p_h}}^2} < \min_{i \in D_h} \frac{\delta_{ih j_h^i}^2}{\tau_{ij_h^i}^2 + \tau_{hj_h^i}^2} \right\} \quad (22)$$

$$S_B = S \setminus S_A \quad (23)$$

$$D_h = \{i | i \in S, p_i = h\} \quad (24)$$

$$D_d = \{h | h \in S_A, p_h = d\} \quad (25)$$

Acknowledgment

This research was supported by the Research Foundation-Flanders, grant number G076815.

References

Andradóttir, S., & Lee, J. S. (2021). Pareto set estimation with guaranteed probability of correct selection. *European Journal of Operational Research*, 292, 286–298.

- Ankenman, B., Nelson, B. L., & Staum, J. (2010). Stochastic kriging for simulation metamodeling. *Operations Research*, *58*, 371–382.
- Applegate, E. A., Feldman, G., Hunter, S. R., & Pasupathy, R. (2020). Multi-objective ranking and selection: Optimal sampling laws and tractable approximations via score. *Journal of Simulation*, *14*, 21–40.
- Auger, A., Bader, J., Brockhoff, D., & Zitzler, E. (2012). Hypervolume-based multiobjective optimization: Theoretical foundations and practical implications. *Theoretical Computer Science*, *425*, 75–103.
- Basseur, M., & Zitzler, E. (2006). A preliminary study on handling uncertainty in indicator-based multiobjective optimization. In *Applications of Evolutionary Computing* (pp. 727–739). Springer Berlin Heidelberg.
- Binois, M., Ginsbourger, D., & Roustant, O. (2015). Quantifying uncertainty on pareto fronts with gaussian process conditional simulations. *European Journal of Operational Research*, *243*, 386–394.
- Boesel, J., Nelson, B. L., & Kim, S.-H. (2003). Using ranking and selection to “clean up” after simulation optimization. *Operations Research*, *51*, 814–825.
- Branke, J., Deb, K., Miettinen, K., & Slowinski, R. (2008). *Multiobjective Optimization: Interactive and Evolutionary Approaches*. Berlin, Heidelberg: Springer-Verlag.
- Branke, J., & Zhang, W. (2019). Identifying efficient solutions via simulation: myopic multi-objective budget allocation for the bi-objective case. *OR Spectrum*, *41*, 831–865.
- Branke, J., Zhang, W., & Tao, Y. (2016). Multiobjective ranking and selection based on hypervolume. In T. Roeder, P. Frazier, R. Szechtman, E. Zhou, T. Huschka, & S. Chick (Eds.), *Proceedings of the 2016 Winter Simulation Conference* (pp. 859–870). Piscataway, New Jersey: IEEE.
- Chen, C.-H., & Lee, L. H. (2010). *Stochastic Simulation Optimization* volume 1. Singapore: World Scientific. doi:10.1142/7437.
- Chen, X., Ankenman, B. E., & Nelson, B. L. (2012). The effects of common random numbers on stochastic kriging metamodels. *ACM Trans. Model. Comput. Simul.*, *22*, 7:1–7:20.
- Chick, S. E., Branke, J., & Schmidt, C. (2010). Sequential sampling to myopically maximize the expected value of information. *INFORMS Journal on Computing*, *22*, 71–80. doi:10.1287/ijoc.1090.0327.
- Cooper, K., & Hunter, S. R. (2020). PyMOSO: software for multiobjective simulation optimization with R-PERLE and R-MinRLE. *INFORMS Journal on Computing*, *32*, 1101–1108.

- Deb, K., Pratap, A., Agarwal, S., & Meyarivan, T. (2002). A fast and elitist multiobjective genetic algorithm: NSGA-II. *IEEE Transactions on Evolutionary Computation*, *6*, 182–197.
- Di Pietro, A., While, L., & Barone, L. (2004). Applying evolutionary algorithms to problems with noisy, time-consuming fitness functions. In *Proceedings of the 2004 Congress on Evolutionary Computation* (pp. 1254–1261). IEEE volume 2.
- Emmerich, M. T., Giannakoglou, K. C., & Naujoks, B. (2006). Single-and multiobjective evolutionary optimization assisted by gaussian random field metamodels. *IEEE Transactions on Evolutionary Computation*, *10*, 421–439.
- Fan, W., Hong, L. J., & Nelson, B. L. (2016). Indifference-zone-free selection of the best. *Operations Research*, *64*, 1499–1514.
- Fawcett, T. (2006). An introduction to ROC analysis. *Pattern recognition letters*, *27*, 861–874.
- Feldman, G., & Hunter, S. R. (2018). Score allocations for bi-objective ranking and selection. *ACM Transactions on Modeling and Computer Simulation*, *28*, 7:1–7:28.
- Feldman, G., Hunter, S. R., & Pasupathy, R. (2015). Multiobjective simulation optimization on finite sets: Optimal allocation via scalarization. In Y. Yilmaz, W. Chan, I. Moon, T. Roeder, C. Macal, & M. Rosseti (Eds.), *Proceedings of the 2015 Winter Simulation Conference (WSC)* (pp. 3610–3621). Piscataway, New Jersey: Institute of Electrical and Electronics Engineers, Inc.
- Fieldsend, J. E., & Everson, R. M. (2005). Multi-objective optimisation in the presence of uncertainty. In *2005 IEEE Congress on Evolutionary Computation* (pp. 243–250). volume 1.
- Fieldsend, J. E., & Everson, R. M. (2015). The rolling tide evolutionary algorithm: A multiobjective optimizer for noisy optimization problems. *IEEE Transactions on Evolutionary Computation*, *19*, 103–117.
- Frazier, P. I. (2014). A fully sequential elimination procedure for indifference-zone ranking and selection with tight bounds on probability of correct selection. *Operations Research*, *62*, 926–942.
- Hernández-Lobato, D., Hernández-Lobato, J. M., Shah, A., & Adams, R. P. (2016). Predictive entropy search for multi-objective bayesian optimization. In *Proceedings of the 33rd International Conference on International Conference on Machine Learning - Volume 48 ICML'16* (pp. 1492–1501). JMLR.
- Hisao Ishibuchi, Noritaka Tsukamoto, & Yusuke Nojima (2008). Evolutionary many-objective optimization: A short review. In *2008 IEEE Congress on Evolutionary Computation (IEEE World Congress on Computational Intelligence)* (pp. 2419–2426).

- Horn, D., Dagge, M., Sun, X., & Bischl, B. (2017). First investigations on noisy model-based multi-objective optimization. In *International Conference on Evolutionary Multi-Criterion Optimization* (pp. 298–313). Springer.
- Huband, S., Hingston, P., Barone, L., & While, L. (2006). A review of multiobjective test problems and a scalable test problem toolkit. *IEEE Transactions on Evolutionary Computation*, *10*, 477–506.
- Hunter, S. R., Applegate, E. A., Arora, V., Chong, B., Cooper, K., Rincón-Guevara, O., & Vivas-Valencia, C. (2019). An introduction to multiobjective simulation optimization. *ACM Trans. Model. Comput. Simul.*, *29*, 7:1–7:36. doi:10.1145/3299872.
- Jalali, H., Van Nieuwenhuysse, I., & Picheny, V. (2017). Comparison of kriging-based algorithms for simulation optimization with heterogeneous noise. *European Journal of Operational Research*, *261*, 279 – 301.
- Jin, Y., & Branke, J. (2005). Evolutionary optimization in uncertain environments—a survey. *IEEE Transactions on evolutionary computation*, *9*, 303–317.
- Kim, S.-H., & Nelson, B. L. (2001). A fully sequential procedure for indifference-zone selection in simulation. *ACM Transactions on Modeling and Computer Simulation (TOMACS)*, *11*, 251–273.
- Kim, S.-H., & Nelson, B. L. (2006). Chapter 17 selecting the best system. In S. G. Henderson, & B. L. Nelson (Eds.), *Simulation* (pp. 501 – 534). Elsevier volume 13 of *Handbooks in Operations Research and Management Science*.
- Kleijnen, J. P. C. (2015). *Design and Analysis of Simulation Experiments*. (2nd ed.). NY: Springer.
- Koch, P., Wagner, T., Emmerich, M. T., Bäck, T., & Konen, W. (2015). Efficient multi-criteria optimization on noisy machine learning problems. *Applied Soft Computing*, *29*, 357–370.
- Law, A. M. (2015). *Simulation Modeling and Analysis*. McGraw-Hill, New York.
- Lee, L. H., Chew, E. P., Teng, S., & Goldsman, D. (2010). Finding the non-dominated pareto set for multi-objective simulation models. *IIE Transactions*, *42*, 656–674.
- Li, M., & Yao, X. (2019). Quality evaluation of solution sets in multiobjective optimisation: A survey. *ACM Computing Surveys*, *52*.
- Miettinen, K. (1999). *Nonlinear multiobjective optimization* volume 12. Springer Science & Business Media.
- Picheny, V., Wagner, T., & Ginsbourger, D. (2013). A benchmark of kriging-based infill criteria for noisy optimization. *Structural and Multidisciplinary Optimization*, *48*, 607–626.

- Ponweiser, W., Wagner, T., Biermann, D., & Vincze, M. (2008). Multiobjective optimization on a limited budget of evaluations using model-assisted s -metric selection. In *International Conference on Parallel Problem Solving from Nature* (pp. 784–794). Springer.
- Powers, D. (2020). Evaluation: from precision, recall and f-measure to roc, informedness, markedness and correlation. *arXiv preprint arXiv:2010.16061*, .
- Rasmussen, C. E., & Williams, C. K. I. (2005). *Gaussian Processes for Machine Learning (Adaptive computation and machine learning)*. (1st ed.). Cambridge, Massachusetts, USA: The MIT Press.
- Rojas-Gonzalez, S., Branke, J., & Nieuwehuysen, I. V. (2019). Multiobjective ranking and selection with correlation and heteroscedastic noise. In *2019 Winter Simulation Conference (WSC)* (pp. 3392–3403).
- Rojas-Gonzalez, S., Jalali, H., & Nieuwenhuysen, I. V. (2020). A multiobjective stochastic simulation optimization algorithm. *European Journal of Operational Research*, *284*, 212 – 226.
- Sacks, J., Welch, W. J., Mitchell, T. J., & Wynn, H. P. (1989). Design and analysis of computer experiments. *Statistical science*, (pp. 409–423).
- Santner, T. J., Williams, B. J., & Notz, W. I. (2013). *The design and analysis of computer experiments*. Springer Science & Business Media.
- Syberfeldt, A., Ng, A., John, R. I., & Moore, P. (2010). Evolutionary optimisation of noisy multi-objective problems using confidence-based dynamic resampling. *European Journal of Operational Research*, *204*, 533–544.
- Teng, S., Lee, L. H., & Chew, E. P. (2010). Integration of indifference-zone with multi-objective computing budget allocation. *European Journal of Operational Research*, *203*, 419 – 429.
- Ting, K. M. (2017). Confusion matrix. *Encyclopedia of Machine Learning and Data Mining*, *260*.
- Trautmann, H., Mehnen, J., & Naujoks, B. (2009). Pareto-dominance in noisy environments. In *Proceedings of the Eleventh Conference on Congress on Evolutionary Computation CEC’09* (pp. 3119–3126). Piscataway, NJ, USA: IEEE Press.
- Voß, T., Trautmann, H., & Igel, C. (2010). New uncertainty handling strategies in multi-objective evolutionary optimization. In *Parallel Problem Solving from Nature, PPSN XI* (pp. 260–269). Berlin, Heidelberg: Springer Berlin Heidelberg.

- Zitzler, E., Brockhoff, D., & Thiele, L. (2007). The hypervolume indicator revisited: On the design of pareto-compliant indicators via weighted integration. In *Evolutionary multi-criterion optimization* (pp. 862–876). Springer.
- Zitzler, E., Knowles, J., & Thiele, L. (2008). Quality assessment of pareto set approximations. *Multiobjective Optimization*, (pp. 373–404).
- Zuluaga, M., Krause, A., & Püschel, M. (2016). ϵ -pal: an active learning approach to the multi-objective optimization problem. *The Journal of Machine Learning Research*, 17, 3619–3650.